

# Eigen and Zundel Forms of Small Protonated Water Clusters: Structures and Infrared Spectra

Mina Park, Ilgyou Shin, N. Jiten Singh, and Kwang S. Kim\*

Center for Superfunctional Materials, Department of Chemistry, Pohang University of Science and Technology, San 31, Hyojadong, Namgu, Pohang 790-784, Korea

Received: May 21, 2007; In Final Form: July 14, 2007

The spectral properties of protonated water clusters, especially the difference between Eigen ( $\text{H}_3\text{O}^+$ ) and Zundel ( $\text{H}_5\text{O}_2^+$ ) conformers and the difference between their unhydrated and dominant hydrated forms are investigated with the first principles molecular dynamics simulations as well as with the high level ab initio calculations. The vibrational modes of the excess proton in  $\text{H}_3\text{O}^+$  are sensitive to the hydration, while those in  $\text{H}_5\text{O}_2^+$  are sensitive to the messenger atom such as Ar (which was assumed to be weakly bound to the water cluster during acquisitions of experimental spectra). The spectral feature around  $\sim 2700\text{ cm}^{-1}$  (experimental value:  $2665\text{ cm}^{-1}$ ) for the Eigen moiety appears when  $\text{H}_3\text{O}^+$  is hydrated. This feature corresponds to the hydrating water interacting with  $\text{H}_3\text{O}^+$ , so it cannot appear in the Eigen core. Thus,  $\text{H}_3\text{O}^+$  alone would be somewhat different from the Eigen forms in water. For the Zundel form (in particular,  $\text{H}_5\text{O}_2^+$ ), there have been some differences in spectral features among different experiments as well as between experiments and theory. When an Ar messenger atom is introduced at a specific temperature corresponding to the experimental condition, the calculated vibrational spectra for  $\text{H}_5\text{O}_2^+\cdot\text{Ar}$  are in good agreement with the experimental infrared spectra showing the characteristic Zundel frequency at  $\sim 1770\text{ cm}^{-1}$ . Thus, the effect of hydration, messenger atom Ar, and temperature are crucial to elucidating the nature of vibrational spectra of Eigen and Zundel forms and to assigning the vibrational modes of small protonated water clusters.

## I. Introduction

Understanding the nature of the excess proton in water is essential for elucidating the large mobility of the proton in water, the acid–base chemistry in solution, and the proton transport in membrane channels.<sup>1</sup> Consequently, the nature of the excess proton has been extensively investigated in both condensed phase and molecular clusters during the past few decades.<sup>2–4</sup> Unlike the O–H stretching of free water molecules, it has been challenging experimentally to detect the vibration modes associated with the proton, because they occur in the low-energy region where it is hard to access in the earlier experimental techniques.<sup>5–9</sup> Despite recent observations of the vibrational spectra involved with the proton motion, the origin of such spectra is not clear because the corresponding theoretical calculations have not properly reproduced the experimental data due to the extremely anharmonic potential surfaces of the systems. Although ab initio calculations have been useful for spectral analysis of clusters,<sup>10</sup> it has shown serious limitations to the study of the excess proton in water clusters even with perturbational anharmonic corrections, because the accurate description of highly anharmonic potential surfaces is practically not feasible. Hence, for such proton-mediated highly anharmonic potentials, first principles Car–Parrinello molecular dynamics (CPMD) simulations<sup>11</sup> have been considered to be very useful to study proton motions such as fluctuation between two limiting forms  $\text{H}_3\text{O}^+$  (Eigen)<sup>12</sup> and  $\text{H}_2\text{O}\cdots\text{H}^+\cdots\text{H}_2\text{O}$  (Zundel).<sup>13</sup> From the previous study of magic  $\text{H}^+(\text{H}_2\text{O})_{21}$  and antimagic  $\text{H}^+(\text{H}_2\text{O})_{22}$  clusters with “on the fly” CPMD simulations,<sup>4</sup> we have found that the results realistically match the experimental observation.<sup>9</sup> Such a simulation method provides important

information about the structural and dynamical interpretation for protonated water species.

In this regard, we have carried out both high level ab initio calculations and first principles CPMD simulations for the  $\text{H}_3\text{O}^+$  [ $\text{H}^+(\text{H}_2\text{O})$ ],  $\text{H}_5\text{O}_2^+$  [ $\text{H}^+(\text{H}_2\text{O})_2$ ],  $\text{H}_5\text{O}_2^+\cdot\text{Ar}$  [ $\text{H}^+(\text{H}_2\text{O})_2\cdot\text{Ar}$ ],  $\text{H}_3\text{O}^+(\text{H}_2\text{O})_3$  [ $\text{H}^+(\text{H}_2\text{O})_4$ ], and  $\text{H}_5\text{O}_2^+(\text{H}_2\text{O})_4$  [ $\text{H}^+(\text{H}_2\text{O})_6$ ] clusters. By simulating two limiting forms,  $\text{H}_3\text{O}^+$  and  $\text{H}_5\text{O}_2^+$ , and their dominant hydrated forms,  $\text{H}_3\text{O}^+(\text{H}_2\text{O})_3$  and  $\text{H}_5\text{O}_2^+(\text{H}_2\text{O})_4$ , we identify the characteristic bands of Eigen or Zundel forms and the hydration effects on the infrared (IR) spectra. Besides, by performing simulations at different temperatures (50/100/150 K) we investigate the thermal and dynamic effects on the vibrational spectra. We also compare  $\text{H}_5\text{O}_2^+\cdot\text{Ar}$  with  $\text{H}_5\text{O}_2^+$  and explain the effect of the Ar messenger atom matrix on spectral features. We indeed find that the vibrational spectrum of Ar-tagged conformer shows a much better agreement with the Ar predissociation IR spectrum of the small protonated water clusters recently reported by Headrick et al.<sup>5</sup> Thus, the present paper analyzes the structures and spectra of the small protonated water clusters, discusses the effects of hydration, messenger atom Ar, and temperature, and elucidates the characteristic features of the Eigen and Zundel forms and these differences.

## II. Computational Methods

We have carried out a series of geometry optimization, frequency analysis, and CPMD simulations on small protonated water clusters. Geometry optimization and harmonic/anharmonic normal mode calculations were carried out using density functional theory (DFT) with the Becke–Lee–Yang–Parr (BLYP) functionals<sup>14</sup> and the corresponding Becke three parameters (B3LYP) and Moller–Plesset second-order perturba-

\* Corresponding author. E-mail: kim@postech.ac.kr.



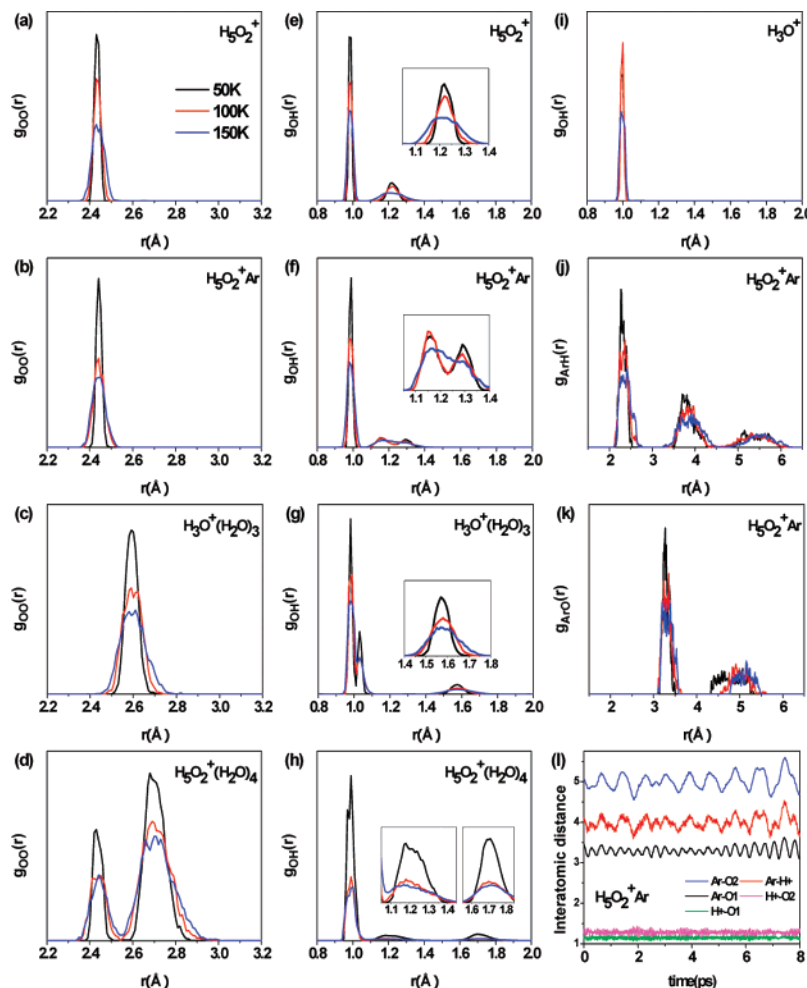


**Figure 2.** Radial distribution functions [ $g_{\text{OO}}$ ,  $g_{\text{OH}}$ ,  $g_{\text{ArH}}$ , and  $g_{\text{ArO}}$ ] of the  $\text{H}_3\text{O}^+$ ,  $\text{H}_5\text{O}_2^+$ ,  $\text{H}_5\text{O}_2^+\text{Ar}$ ,  $\text{H}_3\text{O}^+(\text{H}_2\text{O})_3$ , and  $\text{H}_5\text{O}_2^+(\text{H}_2\text{O})_4$  at 50, 100, and 150 K, and the fluctuation of the interatomic distances for the Ar–O2, Ar–H<sup>+</sup>, Ar–O1, H<sup>+</sup>–O2, and H<sup>+</sup>–O1 of the  $\text{H}_5\text{O}_2^+\text{Ar}$  at 100 K. (black, 50 K; red, 100 K; blue, 150 K).

$\text{H}_5\text{O}_2^+\text{Ar}$ , the O–O distance is 2.43 Å at CCSD(T)/aVDZ, 0.03 Å longer than in  $\text{H}_5\text{O}_2^+$ , and that for the most probable value in  $g_{\text{OO}}$  is 2.45 Å at 150 K (Figure 2b), as in  $\text{H}_5\text{O}_2^+$ . In contrast to the central proton in  $\text{H}_5\text{O}_2^+$ , Figure 1c shows that the central proton in  $\text{H}_5\text{O}_2^+\text{Ar}$  shifts slightly toward the oxygen atom O1 to which the Ar atom is attached (H–O1, 1.11 Å; H–O2, 1.32 Å). Thus, although the Ar atom seems to be attached to the Zundel core H atom, it can also be considered to be attached to the Eigen core. This tendency is also found from two clearly separated peaks of the second band of  $g_{\text{OH}}$  below 100 K in Figure 2f. The distance between Ar and H is 2.31 Å at CCSD(T)/aVDZ. The Ar atom shows slow motion, while the hydrogen atom shows fast oscillation due to their mass difference. By inspecting the fluctuation of interatomic distance between the Ar atom and the proton, the coupled motion is noted in Figure 2l.

$\text{H}_3\text{O}^+(\text{H}_2\text{O})_3$  and  $\text{H}_5\text{O}_2^+(\text{H}_2\text{O})_4$ . As in Figures 1d and 2c,g for  $\text{H}_3\text{O}^+(\text{H}_2\text{O})_3$ , the O–H distance in the central Eigen core is 1.01 Å at the CCSD(T) level and ~1.03 Å in the CPMD simulation (from the second peak of  $g_{\text{OH}}$ , while the first peak of  $g_{\text{OH}}$  appears at 0.98 Å due to the OH distances in three water molecules hydrating the Eigen core). This O–H distance in the central Eigen core is 0.03 Å longer than that in  $\text{H}_3\text{O}^+$ . Such elongation results from the O atoms of the hydrating water molecules pulling out the H atoms of the central Eigen core. In Figures 1e, and 2d,h for the central Zundel core of  $\text{H}_5\text{O}_2^+(\text{H}_2\text{O})_4$ , the O–H distances between the O atoms and the noncentral H atoms are 0.99–1.00 Å, which is also ~0.03 Å longer than

that of  $\text{H}_5\text{O}_2^+$ . The O–O distance of the Zundel core is 2.41 Å at MP2/aVDZ (increased by only 0.01 Å compared with that in  $\text{H}_5\text{O}_2^+$ ) and 2.44 Å at CPMD/150 K (no increase (within 0.01 Å) as compared to that in  $\text{H}_5\text{O}_2^+$ ). Thus, the water molecules in the first hydration shell do not pull out the oxygen atoms in the central Zundel core. The O–H distance in the Zundel core is 1.13 and 1.29 Å at MP2/aVDZ, showing that the proton is not on the center of the two O atoms, in contrast to the case of bare  $\text{H}_5\text{O}_2^+$ . On the other hand, in the CPMD simulation, owing to the temperature effect, the  $g_{\text{OH}}$  shows the broad peak that is near the center of the two Zundel O atoms (at the O–H distance of ~1.2 Å), while the O–H distance fluctuates between 1.1 and 1.35 Å (Figure 2g,l).

For  $\text{H}_3\text{O}^+(\text{H}_2\text{O})_3$ , the O–O distance at CCSD(T)/aVDZ and that at CPMD (for the most probable value in  $g_{\text{OO}}$ ) are about 2.58 and ~2.60 Å, respectively. For  $\text{H}_5\text{O}_2^+(\text{H}_2\text{O})_4$ , (when the O–O distance in the central Zundel core is excluded), the O–O distance between a Zundel O atom and its nearest hydrating water O atoms at MP2/aVDZ and that for the corresponding most probable value in  $g_{\text{OO}}$  at CPMD are 2.65~2.70 and 2.68~2.71 Å, respectively, which are ~0.1 Å longer than the O–O distances in  $\text{H}_3\text{O}^+(\text{H}_2\text{O})_3$ . The OH frequency related to the O–O distance (2.65~2.70 Å) in  $\text{H}_5\text{O}_2^+(\text{H}_2\text{O})_4$  corresponds to the IR frequency of ~3200  $\text{cm}^{-1}$  while that related to the O–O distance (2.58 Å) in  $\text{H}_3\text{O}^+(\text{H}_2\text{O})_3$  corresponds to that of ~2700  $\text{cm}^{-1}$ , which will be discussed in the next section. In the case of  $\text{H}_5\text{O}_2^+(\text{H}_2\text{O})_4$ , because the proton is in between two O atoms, the O–O distance of the Zundel core is shorter and

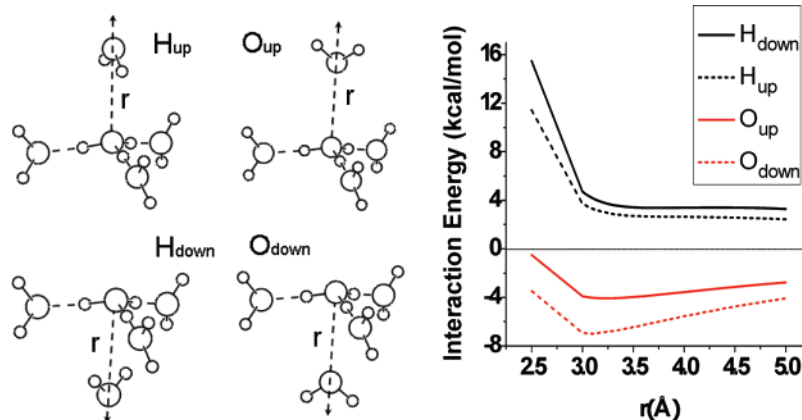


**Figure 3.** Geometries and interaction energies of  $[\text{H}_3\text{O}^+(\text{H}_2\text{O})_3]\text{H}_2\text{O}$  where an extra water molecule is along the  $r$  direction (perpendicular to the molecular cluster plane of trihydrated Eigen core) at the MP2/aVDZ level.

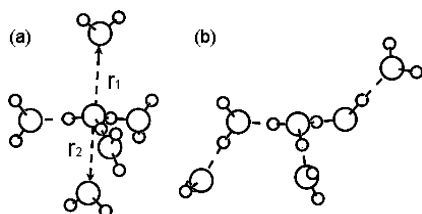


**Figure 4.** MP2/aVDZ optimized geometries of  $\text{H}_2\text{O}[\text{H}_3\text{O}^+(\text{H}_2\text{O})_3]\text{H}_2\text{O}$ .

the non-Zundel O—O distance is longer than the O—O distance of  $\text{H}_3\text{O}^+(\text{H}_2\text{O})_3$ .

Although it is clear that  $\text{H}_3\text{O}^+$  can be easily coordinated by three water molecules by forming  $\text{H}_3\text{O}^+(\text{H}_2\text{O})_3$ , one can wonder whether  $\text{H}_3\text{O}^+$  can be able to have the coordination number up to four or five in solution or in other situations (i.e., the coordination number could be  $3+\epsilon$ ). Thus, we investigated how many additional water molecules could be coordinated to the central Eigen core in  $\text{H}_3\text{O}^+(\text{H}_2\text{O})_3$  and which atom of such water molecules is headed to the Eigen oxygen atom. To this end, we scanned single point MP2/aVDZ energy calculations for two different conformers such that either a hydrogen or an oxygen atom of the additional water molecule is headed to the Eigen core, which were obtained by moving the additional water molecule up or down along the normal direction to the plane made by three oxygen atoms of the dangling water molecules. In Figure 3, which shows the interaction energies depending on the distance ( $r$ ) between two oxygen atoms, we find the favorable  $\text{O}_{\text{up}}$  and  $\text{O}_{\text{down}}$  geometries. Namely, the oxygen atom of the additional water molecule above and below the plane made by three dangling water molecules around the Eigen core is headed to the Eigen core due to the attraction between the excess positive charge of the Eigen core and the dipole moment with the partial negative charge of the oxygen atom in the additional water molecule. The interaction energies between the additional water molecule and  $\text{H}_3\text{O}^+(\text{H}_2\text{O})_3$  for the  $\text{O}_{\text{up}}$  and  $\text{O}_{\text{down}}$  geometries are  $-4.1$  and  $-7.0$  kcal/mol at the MP2/aVDZ level, respectively; those are 16 and 27% of the interaction energy ( $-25.9$  kcal/mol) per each hydrogen bond of the  $\text{H}_3\text{O}^+(\text{H}_2\text{O})_3$ . We also carried out the MP2/aVDZ geometry optimization with two additional water molecules added to the  $\text{H}_3\text{O}^+(\text{H}_2\text{O})_3$  above and below the cluster plane. Both water molecules are  $3.28$  ( $r_1$ ) and  $3.08$  ( $r_2$ ) Å apart from the Eigen oxygen atom as shown in Figure 4a. The interaction energies between the two additional water molecules and the  $\text{H}_3\text{O}^+(\text{H}_2\text{O})_3$  in  $\text{H}_2\text{O}[\text{H}_3\text{O}^+(\text{H}_2\text{O})_3]\text{H}_2\text{O}$  is  $-11.1$  kcal/mol at the MP2/aVDZ level, which is 43% of the average interaction energy for each hydrogen bond in  $\text{H}_3\text{O}^+(\text{H}_2\text{O})_3$ . Therefore, we note that two

additional water molecules whose oxygen atom is headed to the Eigen core can be additionally coordinated to the  $\text{H}_3\text{O}^+(\text{H}_2\text{O})_3$ , and the coordination number of  $\text{H}_2\text{O}[\text{H}_3\text{O}^+(\text{H}_2\text{O})_3]\text{H}_2\text{O}$  could be roughly considered as many as  $3 + 0.43$  in the optimal condition. Of course, in the gas phase, the pentacoordinated Eigen structure spontaneously changes to a more stable tricoordinated Eigen structure with two additional water molecules attached to each first-hydrated water molecule, as shown in Figure 4b.

**B. Vibrational Properties.** We investigated the spectral features of  $\text{H}_3\text{O}^+$ ,  $\text{H}_5\text{O}_2^+$ ,  $\text{H}_5\text{O}_2^+\cdot\text{Ar}$ ,  $\text{H}_3\text{O}^+(\text{H}_2\text{O})_3$ , and  $\text{H}_5\text{O}_2^+(\text{H}_2\text{O})_4$  (Tables 1–5) with the harmonic and anharmonic vibrational analyses of ab initio calculations and with both FT-DACF and FT-VACF of molecular dipole and atomic velocities data respectively of CPMD simulations at 50, 100, and 150 K (Figure 5). The harmonic frequencies at BLYP/aVDZ, BLYP/aVTZ, B3LYP/aVDZ, B3LYP/aVTZ, MP2/aVDZ, MP2/aVTZ, and CCSD(T)/aVDZ levels of theory were scaled by 1.001, 1.000, 0.963, 0.963, 0.957, 0.954, and 0.964, respectively, to match the average value of asymmetric and symmetric stretching frequencies of  $\text{H}_2\text{O}$  ( $3704 \pm 55$ ,  $3706 \pm 51$ ,  $3851 \pm 55$ ,  $3849 \pm 51$ ,  $3873 \pm 67$ ,  $3885 \pm 63$ , and  $3845 \pm 59$   $\text{cm}^{-1}$ , respectively) with the corresponding experimental value ( $3706 \pm 50$   $\text{cm}^{-1}$ ).<sup>23</sup> The effects of the messenger atom Ar and the hydration on the vibrational spectra are particularly studied. In the CPMD simulations, as the BLYP functional is known to systematically underestimate the experimental frequencies we multiplied the vibrational frequencies with scale factors. These scale factors depend on frequencies and can be changed in different systems.<sup>24</sup> In this study, we used the scale factor of 1.025 for  $\text{H}_3\text{O}^+$  and  $\text{H}_5\text{O}_2^+$  and the scale factor of 1.04 for hydrated/solvated Eigen and Zundel cores [ $\text{H}_5\text{O}_2^+\cdot\text{Ar}$ ,  $\text{H}_3\text{O}^+(\text{H}_2\text{O})_3$ , and  $\text{H}_5\text{O}_2^+(\text{H}_2\text{O})_4$ ]. Two different scale factors are because the former is related to the O—H covalent bonds in the protonated species, while the latter involves the noncovalent hydrogen bonds (close to the typical H-bonds) related to the interaction between the H atoms of Eigen/Zundel core and the hydrating water oxygen atoms. For the Zundel system solvated by Ar, we also used the scale factor of 1.04, because the Zundel core behaves partly like an Eigen core interacting with a hydrating water molecule due to the presence of the Ar atom, which shows a partial hydrogen-bonding feature in a protonated system. In this way, the simulated spectra agree very well with the experimental data.

$\text{H}_3\text{O}^+$ ,  $\text{H}_5\text{O}_2^+$ , and  $\text{H}_5\text{O}_2^+\cdot\text{Ar}$ . The experimental asymmetric stretching ( $\nu_3$ ), symmetric stretching ( $\nu_1$ ), and bending frequencies ( $\nu_2$ ) of the water monomer are 3756, 3657, and 1595  $\text{cm}^{-1}$ ,



**TABLE 1: Ab initio Calculated Fundamental Harmonic ( $\omega_h$ ) and Anharmonic ( $\omega_a$ ) Vibrational Frequencies (in  $\text{cm}^{-1}$ ), Spectral Band Peak Positions from CPMD Simulations, and Experimental Infrared Spectra of  $\text{H}_3\text{O}^{+a}$** 

mode <sup>b</sup>	BLYP	B3LYP	MP2		CCSD(T)	CPMD	expt
	$\omega_h$	$\omega_h$	$\omega_h$	$\omega_a$	$\omega_h$	$\omega$ : 150 K [50 K]	w
$\nu_1^c$	3529 <sub>43</sub> (3523)	3514 <sub>47</sub> (3510)	3514 <sub>46</sub> (3515)	3475(3506)	3537	3574 <sub>vw</sub> [ – ] 3534 <sub>w</sub> [3544 <sub>m</sub> ] 3494 <sub>w</sub> [3498 <sub>m</sub> ]	3530 <sup>d</sup> 3514, 3490 <sup>e,f</sup>
$\nu_2$	3425 <sub>3</sub> (3440)	3410 <sub>3</sub> (3426)	3390 <sub>3</sub> (3411)	3368(3415)	3426	3424 <sub>vw</sub> [3428 <sub>w</sub> ]	3390 <sup>f</sup>
$\nu_3^c$	1608 <sub>9</sub> (1640)	1581 <sub>10</sub> (1611)	1599 <sub>9</sub> (1612)	1620(1628)	1620	1628 <sub>s</sub> [1667 <sub>m</sub> ] 1581 <sub>m</sub> [1616 <sub>m</sub> ]	1639 <sup>g</sup> 1626 <sup>g</sup>
$\nu_4$	810 <sub>41</sub> (838)	767 <sub>44</sub> (791)	871 <sub>42</sub> (861)	746(736)	889	768 <sub>s</sub> [770 <sub>s</sub> ]	954, <sup>h</sup> 526

<sup>a</sup> The harmonic frequencies ( $\omega_h$ ) at the BLYP/aVDZ (BLYP/aVTZ), B3LYP/aVDZ (B3LYP/aVTZ), MP2/aVDZ (MP2/aVTZ), and CCSD(T)/aVDZ levels of theory were scaled by 1.001 (1.000), 0.963 (0.963), 0.957 (0.954), and 0.964, respectively, to match the average value of asymmetric and symmetric stretch frequencies of  $\text{H}_2\text{O}$  [3704  $\pm$  55 (3706  $\pm$  51), 3851  $\pm$  55 (3849  $\pm$  51), 3873  $\pm$  67 (3885  $\pm$  63), and 3845  $\pm$  59, respectively] with the corresponding experimental value (3706  $\text{cm}^{-1}$ : ref 22a). The anharmonic frequencies ( $\omega_a$ ) are unscaled values. Values based on the aVTZ basis set are in parentheses. IR intensities are denoted as subscripts in 10 km/mol. Band positions of MD simulation are obtained from the FT-DACF/FT-VACF at 150 K [50 K] (frequencies are scaled by 1.025). The subscripts “s”, “m”, “w”, and “vw” beside frequencies in CPMD and expt (in other tables) denote strong, medium, weak, and very weak (or difficult to resolve), respectively. <sup>b</sup> $\nu_1$ (O–H asym str),  $\nu_2$ (O–H sym str),  $\nu_3$ (H–O–H bend),  $\nu_4$ (H–O–H bend). <sup>c</sup>These frequencies are practically doubly degenerate for ab initio calculations but are split in CPMD simulations at finite temperatures. <sup>d</sup>Ref 25a. <sup>e</sup>Ref 25b. <sup>f</sup>Ref 8d. <sup>g</sup>Ref 25c. <sup>h</sup>Two frequency modes due to the tunneling splitting: ref 25d.

**TABLE 2: Ab initio Calculated Fundamental Harmonic ( $\omega_h$ ) and Anharmonic ( $\omega_a$ ) Vibrational Frequencies (in  $\text{cm}^{-1}$ ), Spectral Band Peak Positions from CPMD Simulations, and Experimental Infrared Spectra of  $\text{H}_5\text{O}_2^{+a}$** 

mode <sup>b</sup>	BLYP	B3LYP	MP2		CCSD(T)	CPMD	expt
	$\omega_h$	$\omega_h$	$\omega_h$	$\omega_a$	$\omega_h$	$\omega$ : 150 K [50 K]	w
$\nu_1$	3684 <sub>27</sub> (3674)	3673 <sub>28</sub> (3664)	3669 <sub>30</sub> (3661)	3641(3663)	3683	3719 <sub>w</sub> [3677 <sub>m</sub> ]	3695, <sup>c</sup> 3693, <sup>d</sup> 3684 <sup>e</sup> 3662, <sup>d</sup> 3660 <sup>e</sup>
$\nu_2$	3594 <sub>0,6</sub> (3596) 3587 <sub>20</sub> (3588)	3585 <sub>0,9</sub> (3587) 3577 <sub>23</sub> (3579)	3567 <sub>0,9</sub> (3569) 3560 <sub>24</sub> (3562)	3552(3583) 3544(3575)	3592 3585	– [3599 <sub>m</sub> ] 3538 <sub>s</sub> [3547 <sub>vw</sub> ]	3617, <sup>d</sup> 3615, <sup>c</sup> 3609 <sup>e</sup> 3528, <sup>d</sup> 3520 <sup>e</sup>
$\nu_3$	1693 <sub>102</sub> (1702) 1625 <sub>0,0</sub> (1647)	1668 <sub>111</sub> (1678) 1599 <sub>0,0</sub> (1619)	1672 <sub>88</sub> (1680) 1619 <sub>0,0</sub> (1627)	1829(1849) 1576(1409)	1690 1643	1720 <sub>s</sub> [1702 <sub>s</sub> ]	1756, <sup>f</sup> 1741 <sup>g</sup>
$\nu_4$	1448 <sub>9</sub> (1478)	1430 <sub>10</sub> (1455)	1461 <sub>10</sub> (1478)	1345(1406)	1484	– [1407–1444 <sub>w</sub> ]	1337, <sup>f</sup> 1317 <sup>g</sup>
$\nu_5$	1393 <sub>25</sub> (1408)	1381 <sub>23</sub> (1397)	1401 <sub>26</sub> (1405)	1309(1348)	1420	1014 <sub>vw</sub> [989 <sub>vw</sub> ]	1163, <sup>f</sup> 1043 <sup>g</sup>
$\nu_6$	974 <sub>261</sub> (983)	874 <sub>271</sub> (891)	774 <sub>290</sub> (868)	545(873)	722	979 <sub>s</sub> [940 <sub>m</sub> ] 887 <sub>vw</sub> [892 <sub>w</sub> ]	990, <sup>f</sup> 921 <sup>g</sup> 788 <sup>g</sup>

<sup>a</sup> See footnote a of Table 1. <sup>b</sup> $\nu_1$ (O–H asym str),  $\nu_2$ (O–H sym str),  $\nu_3$ (H–O–H bend),  $\nu_4$ (O–H<sup>+</sup>–Oy bend),  $\nu_5$ (O–H<sup>+</sup>–Ox bend),  $\nu_6$ (O–H<sup>+</sup>–O asym str). In most cases, the CPMD mode analysis was not needed because the DFT and ab initio modes are already available. When the BLYP/0 K and CPMD/150 K frequencies are significantly different, we used the DACF and VACF analyses, for example, for the O–H–O stretching and bending modes. The OHO bending modes ( $\nu_4$  and  $\nu_5$ ) are coupled in CPMD simulations. The OHO asymmetric stretch ( $\nu_6$ ) assignment has been made using the VACF analysis for the three atoms involving the O–H–O stretching modes, O–H–O bending modes, and the stretching–bending combined O–H–O modes. The three frequencies split around 1000  $\text{cm}^{-1}$  are found to be mainly asymmetric ( $\text{H}_2\text{O}$ )–H–O( $\text{H}_2$ ) stretching modes, while the splitting would be due partly to the constructive, destructive, and insignificant interferences to the O–H–O asymmetric stretching mode by the H atoms of the water molecules. <sup>c</sup>Ref 5 for  $\text{H}_5\text{O}_2^{+}\cdot\text{Ar}$ . <sup>d</sup>Ref 8c for  $\text{H}_5\text{O}_2^{+}\cdot\text{H}_2$ . <sup>e</sup>Ref 8b. <sup>f</sup>Ref 7. <sup>g</sup>Ref 6.

**TABLE 3: Ab Initio Calculated Fundamental Harmonic ( $\omega_h$ ) and Anharmonic ( $\omega_a$ ) Vibrational Frequencies (in  $\text{cm}^{-1}$ ), Spectral Band Peak Positions from CPMD Simulations, and Experimental Infrared Spectra of  $\text{H}_5\text{O}_2^{+}\cdot\text{Ar}^a$** 

mode <sup>b</sup>	BLYP	B3LYP	MP2		CCSD(T)	CPMD <sup>c</sup>	CPMD <sup>d</sup>	expt <sup>e</sup>
	$\omega_h$	$\omega_h$	$\omega_h$	$\omega_a$	$\omega_h$	$\omega$ : 150 K [50 K]	$\omega$ : 150 K [50 K]	w
$\nu_1$	3704 <sub>22</sub> (3692) 3637 <sub>26</sub> (3632)	3630 <sub>25</sub> (3686) 3582 <sub>31</sub> (3622)	3692 <sub>24</sub> (3683) 3615 <sub>37</sub> (3613)	3636(3663) 3635(3645)	3711 3628	3642 <sub>s</sub> [3658 <sub>s</sub> ] 3611 <sub>vw</sub> [ – ]	3695 <sub>s</sub> [3712 <sub>s</sub> ] 3664 <sub>vw</sub> [ – ]	3695 <sub>s</sub> 3660 <sub>s</sub>
$\nu_2$	3608 <sub>9</sub> (3608) 3448 <sub>62</sub> (3441)	3543 <sub>11</sub> (3602) 3476 <sub>59</sub> (3458)	3584 <sub>10</sub> (3585) 3484 <sub>44</sub> (3467)	3597(3579) 3535(3527)	3614 3505	3560 <sub>vw</sub> [ – ] 3437 <sub>s</sub> [3419 <sub>s</sub> ]	3612 <sub>vw</sub> [ – ] 3487 <sub>s</sub> [3469 <sub>s</sub> ]	3615 <sub>w</sub> 3520 <sub>s</sub>
$\nu_3$	1713 <sub>130</sub> (1717) 1626 <sub>0,3</sub> (1648)	1726 <sub>156</sub> (1703) 1670 <sub>0,8</sub> (1619)	1718 <sub>154</sub> (1714) 1621 <sub>0,8</sub> (1630)	1583(1663) 1538(1637)	1761 1645	1727 <sub>s</sub> [1721 <sub>s</sub> ]	1752 <sub>s</sub> [1746 <sub>s</sub> ]	1768 <sub>s</sub>
$\nu_4$	1488 <sub>12</sub> (1516)	1539 <sub>11</sub> (1504)	1516 <sub>15</sub> (1521)	1453(1407)	1550	– [1519 <sub>vw</sub> ]	– [1541 <sub>vw</sub> ]	
$\nu_5$	1344 <sub>24</sub> (1361)	1365 <sub>23</sub> (1335)	1326 <sub>24</sub> (1345)	1242(1111)	1327	– [1350 <sub>vw</sub> ]	– [1370 <sub>vw</sub> ]	
$\nu_6$	1157 <sub>217</sub> (1161)	1094 <sub>197</sub> (1154)	1207 <sub>197</sub> (1195)	– (181)	1300	1091 <sub>s</sub> [1126 <sub>s</sub> ]	1107 <sub>s</sub> [1142 <sub>s</sub> ]	1089 <sub>s</sub>

<sup>a</sup> See footnote a of Table 1. Two very weak shoulder peaks at 925  $\text{cm}^{-1}$  (which might be obtained from the bare  $\text{H}_5\text{O}_2^{+}$ ) and 1872  $\text{cm}^{-1}$  (with unclear origin) are not considered because of their ambiguity. <sup>b</sup> $\nu_1$ (O–H asym str),  $\nu_2$ (O–H sym str),  $\nu_3$ (H–O–H bend),  $\nu_4$ (O–H<sup>+</sup>–Oy bend),  $\nu_5$ (O–H<sup>+</sup>–Ox bend),  $\nu_6$ (O–H<sup>+</sup>–O asym str). <sup>c</sup>Frequencies are scaled by 1.025. <sup>d</sup>Frequencies are scaled by 1.04. This scale factor shows better agreement with experiments. <sup>e</sup>Ref 5.

respectively.<sup>23</sup> These results are reasonably well reproduced from ab initio calculations by using scaled harmonic frequencies or unscaled anharmonic frequencies. Here, to facilitate our

discussion, for the frequency modes of protonated water clusters, we assign the highest frequency mode as  $\nu_1$ , and the lower frequencies  $\nu_n$  in the descending order. For  $\text{H}_3\text{O}^{+}$ , a few

**TABLE 4: Ab Initio Calculated Fundamental Harmonic ( $\omega_h$ ) and Anharmonic ( $\omega_a$ ) Vibrational Frequencies (in  $\text{cm}^{-1}$ ), Spectral Band Peak Positions from CPMD Simulations, and Experimental Infrared Spectra of  $\text{H}_3\text{O}^+(\text{H}_2\text{O})_3^a$** 

mode <sup>b</sup>	BLYP	B3LYP	MP2		CCSD(T)	CPMD	expt
	$\omega_h$	$\omega_h$	$\omega_h$	$\omega_a$	$\omega_h$	$\omega$ : 150 K [50 K]	w
$\nu_1^c$	3744 <sub>34</sub> (3734)	3736 <sub>45</sub> (3726)	3733 <sub>43</sub>	3716	3742	3726 <sub>m</sub> [3729 <sub>m</sub> ]	3730 <sub>s</sub> , <sup>d,e</sup> 3710 <sup>f</sup>
$\nu_2^c$	3645 <sub>6</sub> (3646)	3639 <sub>7</sub> (3639)	3619 <sub>7</sub>	3608	3642	3632 <sub>w</sub> [3634 <sub>vw</sub> ]	3644 <sub>m</sub> , <sup>d,e</sup> 3620 <sup>f</sup>
$\nu_3$	2825 <sub>14</sub> (2832)	2863 <sub>13</sub> (2869)	2880 <sub>17</sub>	2710	2943	2828 <sub>m</sub> [2803 <sub>w</sub> ]	
$\nu_4^c$	2700 <sub>307</sub> (2686)	2758 <sub>304</sub> (2743)	2811 <sub>289</sub>	2686	2864	2771 <sub>s</sub> [2783 <sub>s</sub> ]	2665 <sub>s</sub> <sup>d</sup>
$\nu_5^c$	1633 <sub>3</sub> (1662)	1603 <sub>2</sub> (1634)	1636 <sub>1</sub>	1611	1658	1737 <sub>w</sub> [ - ]	1900 <sub>w</sub> , <sup>d</sup> 1760 <sub>m</sub> <sup>d</sup>
$\nu_6$	1591 <sub>0,0</sub> (1607)	1567 <sub>0,0</sub> (1580)	1568 <sub>0,0</sub>	1600	1592	1607 <sub>w</sub> [1627 <sub>w</sub> ]	1620 <sub>m</sub> <sup>d</sup>
$\nu_7^c$	1565 <sub>3</sub> (1588)	1547 <sub>4</sub> (1567)	1554 <sub>6</sub>	1580	1578		
$\nu_8$	1127 <sub>22</sub> (1164)	1083 <sub>27</sub> (1120)	1151 <sub>23</sub>	987	1161	— [1108 <sub>w</sub> ]	1045 <sub>w</sub> <sup>d</sup>
$\nu_9^c$	970 <sub>6</sub> (956)	949 <sub>5</sub> (934)	931 <sub>7</sub>	892	928	896 <sub>vw</sub> [961 <sub>vw</sub> ]	

<sup>a</sup> See footnote *a* of Table 1. Frequencies from CPMD simulations are scaled by 1.04. <sup>b</sup> $\nu_1$ (O—H asym str of the dangling water molecules),  $\nu_2$ (O—H sym str of the dangling water molecules),  $\nu_3$ (O—H sym str of the Eigen moiety),  $\nu_4$ (O—H asym str of the Eigen moiety),  $\nu_5$ (H—O—H bend of the Eigen moiety (major component) and the dangling water molecules (minor component)),  $\nu_6$ (H—O—H bend of the dangling water molecules),  $\nu_7$ (H—O—H bend of the dangling water molecules and the Eigen moiety, which are almost in equivalent contribution),  $\nu_8$ (H—O—H sym bend in Eigen),  $\nu_9$ (H—O—H asym bend in Eigen). <sup>c</sup>These fundamental frequencies are practically doubly degenerate in ab initio calculations (within 1  $\text{cm}^{-1}$  due to the near  $C_3$  symmetry: E irreducible representation). <sup>d</sup>Ref 5. <sup>e</sup>Ref 8b. <sup>f</sup>Ref 8d.

**TABLE 5: Ab Initio Calculated Fundamental Harmonic ( $\omega_h$ ) and Anharmonic ( $\omega_a$ ) Vibrational Frequencies (in  $\text{cm}^{-1}$ ), Spectral Band Peak Positions from CPMD Simulations, and Experimental Infrared Spectrum of  $\text{H}_5\text{O}_2^+(\text{H}_2\text{O})_4^a$** 

mode <sup>b</sup>	BLYP	B3LYP	MP2	CPMD	expt <sup>d</sup>
	$\omega_h$	$\omega_h$	$\omega_h$	$\omega$ : 150 K [50 K]	w
$\nu_1^c$	3750 <sub>7</sub> (3742)	3743 <sub>10</sub> (3736)	3742 <sub>12</sub>	3723 <sub>m</sub> [3728 <sub>m</sub> ]	3740 <sub>s</sub>
$\nu_2^c$	3650 <sub>5</sub> (3652)	3646 <sub>4</sub> (3648)	3626 <sub>4</sub>	3631 <sub>m</sub> [3636 <sub>m</sub> ]	3650 <sub>m</sub>
$\nu_3$	3184 <sub>2</sub> (3189)	3235 <sub>7</sub> (3224)	3326 <sub>147</sub>	3282 <sub>s</sub> [3263 <sub>s</sub> ]	3250 <sub>vw</sub>
$\nu_4$	3167 <sub>154</sub> (3163)	3187 <sub>164</sub> (3205)	3151 <sub>190</sub>		
	3170 <sub>240</sub> (3165)	3227 <sub>236</sub> (3208)	3280 <sub>46</sub>	3189 <sub>s</sub> [ - ]	
	3146 <sub>95</sub> (3153)	3174 <sub>71</sub> (3189)	3135 <sub>77</sub>	3145 <sub>s</sub> [3201 <sub>s</sub> ]	3160 <sub>s</sub>
$\nu_5$	1692 <sub>59</sub> (1707)	1671 <sub>71</sub> (1683)	1701 <sub>87</sub>	1773 <sub>s</sub> [1738 <sub>s</sub> ]	1770 <sub>s</sub>
	1652 <sub>0,5</sub> (1676)	1628 <sub>0,5</sub> (1653)	1659 <sub>0,9</sub>		
$\nu_6^c$	1584 <sub>9</sub> (1601)	1561 <sub>8</sub> (1576)	1560 <sub>7</sub>	— [1623 <sub>m</sub> ]	1620 <sub>m</sub>
$\nu_7$	1511 <sub>4</sub> (1546)	1500 <sub>5</sub> (1533)	1539 <sub>12</sub>		
$\nu_8$	1392 <sub>16</sub> (1410)	1371 <sub>16</sub> (1385)	1360 <sub>21</sub>		
$\nu_9$	985 <sub>240</sub> (994)	943 <sub>208</sub> (947)	1153 <sub>310</sub>	1055 <sub>s</sub> [967 <sub>s</sub> ]	1055 <sub>s</sub>

<sup>a</sup> See footnote *a* of Table 1. Frequencies from CPMD simulations are scaled by 1.04. <sup>b</sup> $\nu_1$ (O—H asym str in dangling water),  $\nu_2$ (O—H sym str in dangling water),  $\nu_3$ (O—H asym str in Zundel),  $\nu_4$ (O—H sym str in Zundel),  $\nu_5$ (H—O—H bend in Zundel),  $\nu_6$ (H—O—H bend in dangling water),  $\nu_7$ (O—H<sup>+</sup>—O<sub>y</sub> bend),  $\nu_8$ (O—H<sup>+</sup>—O<sub>x</sub> bend),  $\nu_9$ (O—H<sup>+</sup>—O asym str). <sup>c</sup>These fundamental frequencies are practically quadruply degenerate in ab initio calculations. <sup>d</sup>Ref 5.

experiments<sup>8d,25</sup> observed a few different regions, reporting the asymmetric stretching frequencies ( $\nu_1$ ) around 3530 and 3514/3490  $\text{cm}^{-1}$ , the symmetric stretching frequencies ( $\nu_2$ ) at 3390  $\text{cm}^{-1}$ , the bending frequencies ( $\nu_3$ ) at 1639 and 1626  $\text{cm}^{-1}$ , and another bending frequencies ( $\nu_4$ ) at 954 and 526  $\text{cm}^{-1}$ . Ab initio calculations show two degenerate peaks at  $\nu_1$  and  $\nu_3$ , while CPMD simulations show two (or a few) split frequencies for  $\nu_1$  and two split frequencies for  $\nu_3$  due to anharmonic couplings. For  $\nu_1$ , the experimental two split peaks (3530 and 3514/3490  $\text{cm}^{-1}$ ) are in good agreement with the CPMD two split frequencies (3544 and 3498  $\text{cm}^{-1}$  at 50 K; 3534 and 3494  $\text{cm}^{-1}$  at 150 K; the very weak frequency 3574  $\text{cm}^{-1}$  at 150 K does not need to be considered) and also with the degenerate ab initio frequencies ( $\sim 3500 \text{ cm}^{-1}$ ). The experimental  $\nu_2$  (3390  $\text{cm}^{-1}$ ) is in good agreement with the CPMD  $\nu_2$  (3424/3428  $\text{cm}^{-1}$  at 150/50 K) and with the ab initio  $\nu_2$  ( $\sim 3400 \text{ cm}^{-1}$ ). The experimental two split  $\nu_3$  (1639 and 1626  $\text{cm}^{-1}$ ) are in reasonable agreement with the CPMD two split frequencies (1628/1667 and 1581/1616  $\text{cm}^{-1}$  at 150/50 K) and with the ab initio degenerate frequencies ( $\sim 1600 \text{ cm}^{-1}$ ). For  $\nu_4$ , the experiment shows two frequencies due to the tunneling splitting (954 and 526  $\text{cm}^{-1}$ ),<sup>7</sup> while the CPMD and ab initio calculations ( $\sim 800 \text{ cm}^{-1}$ ) did not consider such splitting.

For the clusters having the Zundel moiety, there has been a long argument about the assignment of the bridging proton

oscillation mode around 1000  $\text{cm}^{-1}$ . Regarding the protonated water dimer,<sup>5–8</sup> Asmis et al.<sup>6</sup> observed 921, 1043, 1317, and 1741  $\text{cm}^{-1}$ ; Fridgen et al.<sup>7</sup> assigned the bands centered at 990, 1163, 1337, and 1756  $\text{cm}^{-1}$  to the O—H<sup>+</sup>—O stretching mode and H—O—H bending mode; Headrick et al.<sup>5</sup> observed 1089  $\text{cm}^{-1}$  and 1768  $\text{cm}^{-1}$  for  $\text{H}_5\text{O}_2^+\cdot\text{Ar}$  at a low temperature. These experiments show a broad band (with a few peaks) around  $\sim 1000 \text{ cm}^{-1}$  and a unique Zundel peak around  $\sim 1750 \text{ cm}^{-1}$ . A number of theoretical studies of  $\text{H}_5\text{O}_2^+$  have been carried out.<sup>26</sup> However, the clear assignment of the Zundel form still needs to be made, as experimental values vary depending on the experimental condition. As shown in the of  $\text{H}_5\text{O}_2^+$  spectra of Table 2, the O—H asymmetric stretch mode ( $\nu_1$ ) appears at  $\sim 3690$  and  $\sim 3660 \text{ cm}^{-1}$  in experiments, 3719/3677  $\text{cm}^{-1}$  at 150/50 K simulations, and  $\sim 3680 \text{ cm}^{-1}$  for ab initio calculations. The O—H symmetric stretch mode ( $\nu_2$ ) appears at  $\sim 3615$  and  $\sim 3525 \text{ cm}^{-1}$  in experiments, 3599/3538  $\text{cm}^{-1}$  in 50/150 K simulations, and  $\sim 3590$  and  $\sim 3580 \text{ cm}^{-1}$  in ab initio calculations. The H—O—H bending mode ( $\nu_3$ ) appears at  $\sim 1750 \text{ cm}^{-1}$  in experiments, 1720/1702  $\text{cm}^{-1}$  in 150/50 K simulations, and  $\sim 1690 \text{ cm}^{-1}$  (strong intensity) in ab initio calculations, while another H—O—H bending mode ( $\nu_3$ ) around  $\sim 1640 \text{ cm}^{-1}$  in ab initio calculations shows almost zero intensity. The two O—H<sup>+</sup>—O bending modes ( $\nu_4$  and  $\nu_5$ ) with weak intensity appear around  $\sim 1450$  and  $\sim 1400 \text{ cm}^{-1}$  for 50 K simulations

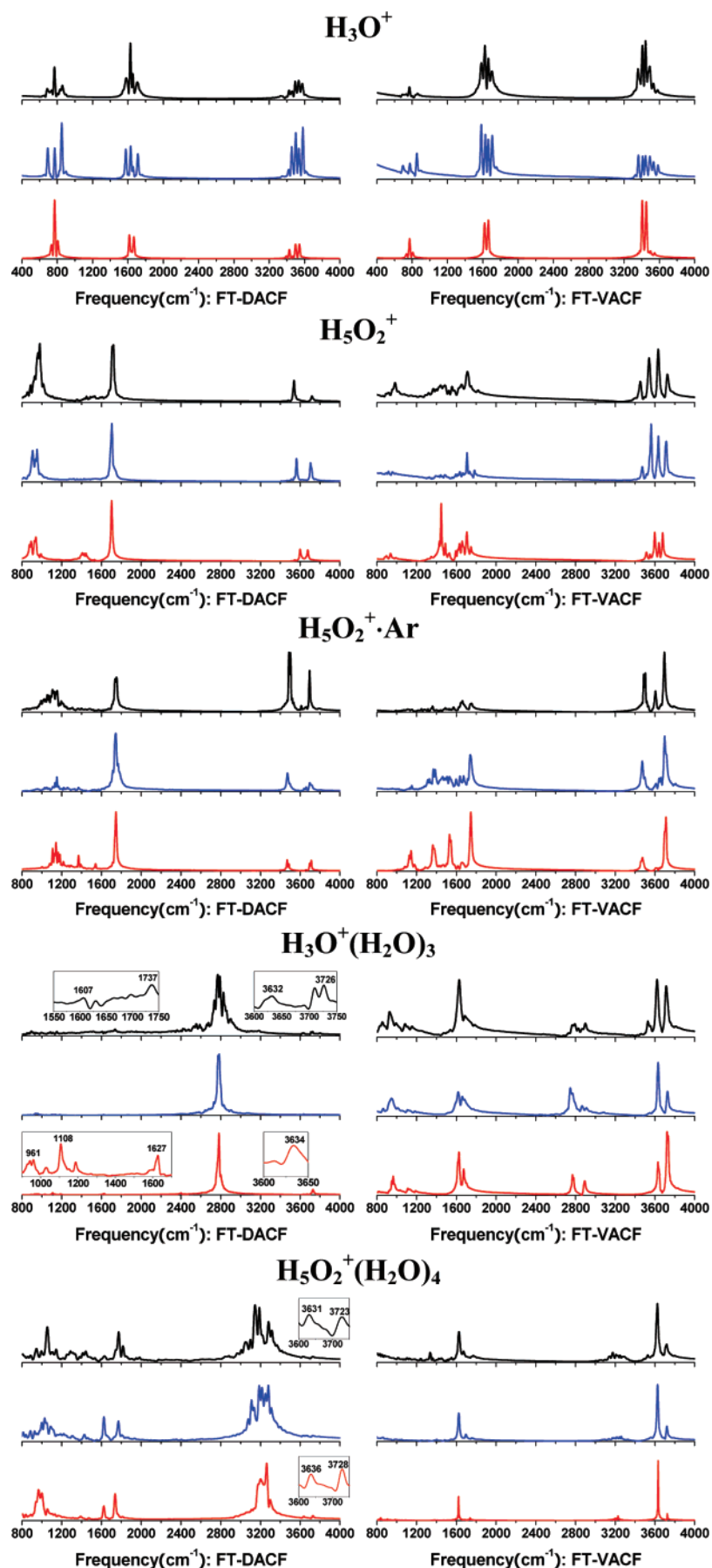


**Figure 5.** FT-DACF (left) and FT-VACF (right) of  $\text{H}_3\text{O}^+$ ,  $\text{H}_5\text{O}_2^+$ ,  $\text{H}_5\text{O}_2^+\cdot\text{Ar}$ ,  $\text{H}_3\text{O}^+(\text{H}_2\text{O})_3$ , and  $\text{H}_5\text{O}_2^+(\text{H}_2\text{O})_4$  at 50, 100, and 150 K (with first/red, second/blue, and third/black lines from below, respectively).

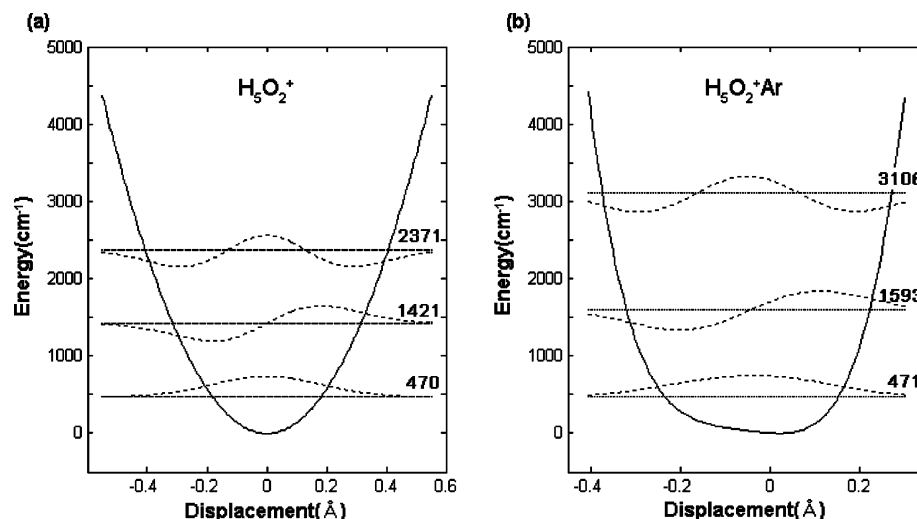


Figure 6. Potential energy curves and vibrational energy levels of (a)  $\text{H}_5\text{O}_2^+$  and (b)  $\text{H}_5\text{O}_2^+\cdot\text{Ar}$

and ab initio calculations. However, above 100 K, the two peaks almost disappear. For the O–H<sup>+</sup>–O asymmetric stretching mode ( $\nu_6$ ), ab initio calculations predict a peak around 700–1000  $\text{cm}^{-1}$  (depending on the level of theory), and the 150 K simulation shows a peak around  $\sim 980\text{ cm}^{-1}$ , while the 50 K simulation gives a medium peak around  $\sim 940$ , a weak peak around  $\sim 890$ , and a very weak peak around  $\sim 990\text{ cm}^{-1}$ . The experimental peaks around  $\sim 1000\text{ cm}^{-1}$  were observed at 788, 921, 1043, and  $1317\text{ cm}^{-1}$  by Asmis et al. and at 990, 1163, and  $1337\text{ cm}^{-1}$  by Fridgen et al. It is not clear to us whether the frequency of  $1317/1337\text{ cm}^{-1}$  would correspond to the O–H<sup>+</sup>–O bending modes ( $\nu_4$  and  $\nu_5$ ) around  $\sim 1400\text{ cm}^{-1}$ . All calculations show that a broad band (with a few peaks) is around  $\sim 950\text{ cm}^{-1}$  and a unique Zundel peak is around  $\sim 1750\text{ cm}^{-1}$ , which agrees with experiments. The broad frequency band (with a few peaks) around  $\sim 950\text{ cm}^{-1}$  is somewhat off the experimental frequency  $1089\text{ cm}^{-1}$  observed for  $\text{H}_5\text{O}_2^+\cdot\text{Ar}$  by Headrick et al. Thus, the effect of an Ar messenger atom on the  $\text{H}_5\text{O}_2^+$  spectra needs to be investigated.

In the case of  $\text{H}_5\text{O}_2^+\cdot\text{Ar}$ , the O–H asymmetric stretch mode ( $\nu_1$ ) appears with two split peaks at  $3695$  and  $3660\text{ cm}^{-1}$  in experiments. These are well reproduced in the 150 K CPMD simulation, which shows two split peaks at  $3695$  and  $3664\text{ cm}^{-1}$ , while ab initio calculations show a degenerate peak around  $\sim 3700\text{ cm}^{-1}$ . The O–H symmetric stretch mode ( $\nu_2$ ) appears at  $3615$  and  $3520\text{ cm}^{-1}$  in experiments,  $3612$  and  $3487\text{ cm}^{-1}$  in the 150 K simulation, and  $\sim 3600$  and  $\sim 3500\text{ cm}^{-1}$  in ab initio calculations. The H–O–H bending mode ( $\nu_3$ ) with strong intensity appears at  $1768\text{ cm}^{-1}$  in experiments,  $1752\text{ cm}^{-1}$  in the 150 K simulation, and  $\sim 1700\text{ cm}^{-1}$  in ab initio calculations, while another weak H–O–H bending mode ( $\nu_3$ ) shows almost zero intensity, as can be noted from the ab initio frequency around  $\sim 1640\text{ cm}^{-1}$  as well as the disappearance of such a peak in the 150 K simulation. The two O–H<sup>+</sup>–O bending modes ( $\nu_4$  and  $\nu_5$ ) with weak intensity appear around  $\sim 1540$  and  $\sim 1370\text{ cm}^{-1}$  for the 50 K simulations but disappear above 100 K. These modes appear at  $1500$  and  $1300\text{ cm}^{-1}$  with weak intensity in ab initio calculations. The O–H<sup>+</sup>–O asymmetric stretching mode ( $\nu_6$ ) appears at  $1089\text{ cm}^{-1}$  in experiments,  $1107\text{ cm}^{-1}$  in the 150 K simulation, and  $\sim 1200\text{ cm}^{-1}$  in ab initio calculations.

Although anharmonic frequencies involving coupling between modes are properly taken into account in CPMD simulations, the scaling method in ab initio calculations is not physically sound, and the low-order anharmonic perturbation correction

method is not reliable to describe the proton-oscillating mode for  $\text{H}_5\text{O}_2^+$  and  $\text{H}_5\text{O}_2^+\cdot\text{Ar}$ . In this regard, to correctly understand the Ar messenger effect in ab initio calculations, we must obtain accurate frequencies for the proton-oscillating asymmetric stretching mode ( $\nu_6$ ) for both  $\text{H}_5\text{O}_2^+$  and  $\text{H}_5\text{O}_2^+\cdot\text{Ar}$ . Thus, we studied the potential energy surfaces of both  $\text{H}_5\text{O}_2^+$  and  $\text{H}_5\text{O}_2^+\cdot\text{Ar}$ , as shown in Figure 6. The CCSD(T)/aVTZ single point energy calculations were carried out at several geometries that were obtained by moving the proton in the Zundel ion along the normal mode direction at the MP2/aVTZ optimized geometries. The potential energy curves were fitted in Taylor series, and the one-dimensional Schrödinger equation was numerically solved.<sup>27</sup> The calculated eigenvalues corresponding to the three lowest vibrational modes of the  $\text{H}_5\text{O}_2^+$  are  $E_0 = 470$  and  $E_1 = 1421\text{ cm}^{-1}$ . Thus, the fundamental vibrational frequency of the  $\nu_6$  mode is  $951\text{ cm}^{-1}$ , similar to the simulated frequencies ( $979/940\text{ cm}^{-1}$  150/50 K) for  $\text{H}_5\text{O}_2^+$ . On the other hand, the eigenvalues of  $\text{H}_5\text{O}_2^+\cdot\text{Ar}$  corresponding to the three lowest vibrational modes are  $E_0 = 471$  and  $E_1 = 1593\text{ cm}^{-1}$ , so that the lowest vibrational frequency mode  $\nu_6$  is  $1122\text{ cm}^{-1}$ .

From the CPMD simulations of the Ar-tagged conformer as compared to  $\text{H}_5\text{O}_2^+$ , the  $\nu_1$  mode is significantly blue-shifted from  $979$  to  $1091/1107\text{ cm}^{-1}$  at 150 K and from  $940$  to  $1126/1142\text{ cm}^{-1}$  at 50 K at the FT-DACF spectra, in agreement with experiments (from  $921/990$  to  $1089\text{ cm}^{-1}$ ) as well as the CCSD(T)/aVTZ/MP2/aVTZ frequency analysis of the  $\nu_6$  mode (from  $951$  to  $1122\text{ cm}^{-1}$ ). From these spectral analyses, we note that the messenger atom Ar shows a significant shift in the frequency of the  $\nu_6$  mode. This is actually expected because the central proton in  $\text{H}_5\text{O}_2^+\cdot\text{Ar}$  is not near the center of the two O atoms; thus, although the Ar atom seems to be attached to the Zundel core H atom, it can also be partly considered to be attached to the Eigen core, which is contrasted to the pure Zundel form of  $\text{H}_5\text{O}_2^+$ . The  $\nu_3$  mode is slightly blue-shifted from  $1720$  to  $1727/1752\text{ cm}^{-1}$  at 150 K and from  $1702$  to  $1721/1746\text{ cm}^{-1}$  at 50 K due to the Ar tagging, consistent with the experiments (from  $1741/1756$  to  $1768\text{ cm}^{-1}$ ). Thus, the Ar-tagging effect explains some differences in frequencies among different experimental conditions.

$\text{H}_3\text{O}^+(\text{H}_2\text{O})_3$  and  $\text{H}_5\text{O}_2^+(\text{H}_2\text{O})_4$ . In the case of  $\text{H}_3\text{O}^+(\text{H}_2\text{O})_3$ , the hydration shell makes the O–H asymmetric and symmetric modes and H–O–H bending modes blue-shifted as compared with the bare  $\text{H}_3\text{O}^+$ . In addition, more complicated bending modes appear, and the characteristic O–H stretching modes of



the Eigen core appear. The O–H asymmetric and symmetric stretch modes ( $\nu_1$  and  $\nu_2$ ) appear at (3730/3710 and 3644/3620  $\text{cm}^{-1}$ ) in experiments, (3726/3729 and 3632/3634  $\text{cm}^{-1}$ ) at 150/50 K simulations, and ( $\sim 3740$  and  $\sim 3640$   $\text{cm}^{-1}$ ) in ab initio calculations. The O–H symmetric stretch frequency ( $\nu_3$ ) around  $\sim 2820$   $\text{cm}^{-1}$  (difficult to be resolved from the strong peak at  $\sim 2771$   $\text{cm}^{-1}$ ) was not observed in experiments. On the other hand, the characteristic strong O–H asymmetric stretch frequency ( $\nu_4$ ) at 2771/2783  $\text{cm}^{-1}$  in 150/50 K simulations and at  $\sim 2800$   $\text{cm}^{-1}$  in ab initio calculations was observed at 2665  $\text{cm}^{-1}$  in experiments. The weak H–O–H bending modes ( $\nu_5$  and  $\nu_6$ ) appear (1760 and 1620  $\text{cm}^{-1}$ ) in experiments, (1737 and 1607/1627  $\text{cm}^{-1}$ ) in 150/50 K simulations, and ( $\sim 1650$  and  $\sim 1590$   $\text{cm}^{-1}$ ) in ab initio calculations. A weak H–O–H symmetric-bending frequency ( $\nu_8$ ) appears at 1045  $\text{cm}^{-1}$  in experiments, 1108  $\text{cm}^{-1}$  in 50 K simulations, and  $\sim 1150$   $\text{cm}^{-1}$  in ab initio calculations. Other very weak H–O–H bending modes ( $\nu_7$  at  $\sim 1580$   $\text{cm}^{-1}$  and  $\nu_9$  at  $\sim 900$   $\text{cm}^{-1}$ ) were not observed in experiments.

In the case of  $\text{H}_3\text{O}^+(\text{H}_2\text{O})_3$ , the origin of the frequencies at 1760 and 1900  $\text{cm}^{-1}$  is not clear. It is known that the band near 1760  $\text{cm}^{-1}$  indicates Zundel moieties, which is evidenced from such a peak at the experimental IR spectra of  $\text{H}_5\text{O}_2^+$  and  $\text{H}_5\text{O}_2^+(\text{H}_2\text{O})_4$  conformers. This peak is observed near 1722 and 1744  $\text{cm}^{-1}$  in the MD simulations of  $\text{H}_5\text{O}_2^+\cdot\text{Ar}$  and  $\text{H}_5\text{O}_2^+(\text{H}_2\text{O})_4$ , respectively, which will be discussed later. Thus, the experimental peak near 1760  $\text{cm}^{-1}$  could indicate the probabilistic appearance of Zundel moiety resulted from the fluctuation of the hydrogen atoms in the Eigen core arisen from some of nonequilibrated hot clusters. Meanwhile, the experimental vibrational peak near 1900  $\text{cm}^{-1}$  is unclear to us because they are not observed from ab initio-calculated and CPMD-simulated spectra. We do not exclude a possibility that such peaks could arise from a low-lying energy isomer that could be stable at somewhat high temperatures.

Like  $\text{H}_3\text{O}^+(\text{H}_2\text{O})_3$ , in the case of  $\text{H}_5\text{O}_2^+(\text{H}_2\text{O})_4$  the hydration shell makes the O–H asymmetric and symmetric modes and H–O–H-bending modes blue-shifted as compared with the bare  $\text{H}_5\text{O}_2^+$ . The O–H asymmetric and symmetric stretch modes ( $\nu_1$  and  $\nu_2$ ) appear at (3740 and 3650  $\text{cm}^{-1}$ ) in experiments, (3723/3728 and 3631/3636  $\text{cm}^{-1}$ ) at 150/50 K simulations, and ( $\sim 3740$  and  $\sim 3640$   $\text{cm}^{-1}$ ) in ab initio calculations. These outershell water molecular frequencies are almost the same with those of  $\text{H}_3\text{O}^+(\text{H}_2\text{O})_3$ . The O–H asymmetric stretch frequencies ( $\nu_3$ ) are very weak at  $\sim 3250$   $\text{cm}^{-1}$  in experiments, 3282/3263 in 150/50 K simulations, and  $\sim 3200$   $\text{cm}^{-1}$  in ab initio calculations. The O–H symmetric stretch frequency ( $\nu_4$ ) appears strongly at 3160  $\text{cm}^{-1}$  in experiments, 3145/3201  $\text{cm}^{-1}$  in 150/50 K simulations, and  $\sim 3150$   $\text{cm}^{-1}$  in ab initio calculations. The strong H–O–H bending modes of the Zundel core ( $\nu_5$ ) appears at 1770  $\text{cm}^{-1}$  in experiments, 1733/1738  $\text{cm}^{-1}$  in 150/50 K simulations, and  $\sim 1700$   $\text{cm}^{-1}$  in ab initio calculations, while the very weak peak around  $\sim 1650$   $\text{cm}^{-1}$  is not observed in experiments and CPMD simulations. The H–O–H bending mode ( $\nu_6$ ) appears 1620  $\text{cm}^{-1}$  in experiments, 1623  $\text{cm}^{-1}$  in 50 K simulations, and  $\sim 1570$   $\text{cm}^{-1}$  in ab initio calculations. Very weak O–H $^+$ –O-bending frequencies ( $\nu_7$  and  $\nu_8$ ) at  $\sim 1510$  and  $\sim 1370$   $\text{cm}^{-1}$  in ab initio calculations are not observed in both experiments and CPMD simulations. The O–H $^+$ –O asymmetric stretching frequency ( $\nu_9$ ) appears at 1055  $\text{cm}^{-1}$  in experiments, 1055/967  $\text{cm}^{-1}$  in 150/50 K simulations, and  $\sim 1000$   $\text{cm}^{-1}$  in ab initio calculations.

On the basis of the MD simulation for  $\text{H}_5\text{O}_2^+(\text{H}_2\text{O})_4$ , most vibrational modes of  $\text{H}_5\text{O}_2^+$  are slightly blue-shifted except for

the new O–H stretching modes of the water molecules in the central Zundel ion. At the CPMD/150 K simulations, although the intensities of the broad  $\nu_3$  (3282  $\text{cm}^{-1}$ ) and  $\nu_4$  (3145  $\text{cm}^{-1}$ ) bands are strong the intensities of both O–H asymmetric-stretching  $\nu_1$  (3723  $\text{cm}^{-1}$ ) and symmetric  $\nu_2$  (3631  $\text{cm}^{-1}$ ) modes of the free water molecules in the first hydration shell are weak (Figure 5). On the basis of our assessment of the predicted temperature-dependent spectra in terms of the overall agreements with the experimental data, we estimate the experimental temperature to be 100–150 K (for example, the O–H symmetry-stretching frequency at 150 K (3145  $\text{cm}^{-1}$ ) is close to the experimental value (3160  $\text{cm}^{-1}$ )).

As discussed above, we have observed realistic frequencies based on the CPMD simulations, which are in good agreement with experiments. Although the energy barrier of the CPMD potential tends to be lower than the more accurate ab initio results, the underestimation of the CPMD potential barriers is likely to partially reflect the quantum-tunneling driven effective barriers for the accurate potential surface and would give more realistic simulation results, as noted in our previous simulation study of the magic- and antimagic-protonated water clusters.<sup>4</sup>

#### IV. Concluding Remarks

We have investigated the spectral features of small protonated water clusters, Eigen core ( $\text{H}_3\text{O}^+$ ), Zundel core ( $\text{H}_5\text{O}_2^+$ ), Zundel core solvated by Ar ( $\text{H}_5\text{O}_2^+\cdot\text{Ar}$ ), hydrated Eigen core [ $\text{H}_3\text{O}^+(\text{H}_2\text{O})_3$ ], and hydrated Zundel core [ $\text{H}_5\text{O}_2^+(\text{H}_2\text{O})_4$ ]. Our special attention has been focused on the proton motions based on ab initio calculations and CPMD simulations. By comparing the bare Eigen and Zundel cores with their dominant hydrated/solvated conformers, we investigated the hydration/solvation effect on the characteristic vibrational peaks of Eigen or Zundel forms. The characteristic Eigen frequency (H–O–H bending between the OH of hydrating water molecules and the H atom in Eigen core) is  $\sim 2700$   $\text{cm}^{-1}$ , which arises from the interaction between the Eigen core and the hydrating water molecules. Thus, this unique feature cannot be seen for the Eigen core alone. One can easily note that the coordination number of the Eigen core has clearly three in the gas phase, but it could be increased up to  $\sim 3.4$  when it is fully hydrated, because the O atoms of the additional hydrating water molecules above and below the molecular cluster plane of trihydrated Eigen core are likely to be headed to the positively charged Eigen core.

From the study of  $\text{H}_5\text{O}_2^+$  and  $\text{H}_5\text{O}_2^+\cdot\text{Ar}$  clusters, we find the significant effect of the messenger atom Ar on the proton position/motion and the relevant vibrational frequency. In the Zundel core solvated by the messenger atom Ar, the central proton shifts its position toward to the O atom to which the Ar atom is attached, resulting in breaking the quasi- $C_2$  symmetry of the bare  $\text{H}_5\text{O}_2^+$  structure. Thus, both ab initio-calculated and CPMD-simulated vibrational spectra of the Ar-tagged conformer  $\text{H}_5\text{O}_2^+\cdot\text{Ar}$  are significantly different from those of the bare  $\text{H}_5\text{O}_2^+$ . For the CPMD simulations of the Ar-tagged conformer, the O–H $^+$ –O asymmetric stretch mode is significantly blue-shifted from 979 to 1091/1107  $\text{cm}^{-1}$  at 150 K, which is in agreement with experiments (from 921/990 to 1089  $\text{cm}^{-1}$ ). This shift can be also understood from the anharmonicity-driven vibrational frequency change (951 to 1122  $\text{cm}^{-1}$ ) based on the CCSD(T)/aVTZ//MP2/aVTZ potential energy surface. The unique Zundel frequency (H–O–H bending mode) is  $\sim 1750$   $\text{cm}^{-1}$ . By Ar-tagging, this frequency is slightly blue-shifted (from 1720 to 1727/1752  $\text{cm}^{-1}$  at the CPMD/150 K simulation), which is consistent with experiments (from 1741/1756 to 1768  $\text{cm}^{-1}$ ). Thus, the significant effect of an Ar messenger atom on

the  $\text{H}_5\text{O}_2^+$  spectra around  $\sim 1000$  and  $\sim 1750\text{ cm}^{-1}$  is due to the structural change from the pure Zundel form of  $\text{H}_5\text{O}_2^+$  to the Zundel–Eigen hybrid form of  $\text{H}_5\text{O}_2^+\cdot\text{Ar}$  by the symmetry breaking of the structure in the presence of an Ar atom. As the potential surface with respect to the proton motion is highly anharmonic, the temperature effect is also not small on the spectra. All these effects explain the differences in spectra among different experimental conditions. The spectrum of  $\text{H}_5\text{O}_2^+$  without Ar matches well with the experimental results of Asmis et al. and Fridgen et al. while that with a tagged Ar matches well with the experimental results of Headrick et al.<sup>5–7</sup>

The O–H stretching vibrational modes of the Eigen and Zundel cores are generally blue-shifted in their hydrated clusters due to the interaction with the hydrating water molecules. As the temperature increases, some peaks are either broadened or disappeared. To sum up, by taking into account the effects of hydration, messenger Ar atom, and temperature, we were able to realistically reproduce the experimental IR spectra and elucidate the nature of the characteristic features of Eigen and Zundel forms except for very few unclearly resolved experimental frequencies.

**Acknowledgment.** This paper has been dedicated to Prof. Fumio Hirata, who has been a long-time friend of mine, for his 60th birthday. This work was supported by the Brain Korea 21 program and Global Research Laboratory (GRL) program of KICOS. Most calculations were performed with supercomputers at KISTI.

**Supporting Information Available:** The unscaled frequencies of Tables 1–5. This material is available free of charge via the Internet at <http://pubs.acs.org>.

## References and Notes

- (1) (a) Kornyshev, A. A.; Kuznetsov, A. M.; Spohr, E.; Ulstrup, J. J. *Phys. Chem. B* **2003**, *107*, 3351. (b) Duff, K. D.; Ashley, R. H. *Virology* **1992**, *190*, 485. (c) Pomes, R.; Roux, B. *J. Phys. Chem.* **1996**, *100*, 2519.
- (2) (a) Geissler, P. L.; Dellago, C.; Chandler, D.; Hutter, J.; Parrinello, M. *Science* **2001**, *291*, 2121. (b) Marx, D.; Tuckermann, M. E.; Hutter, J.; Parrinello, M. *Nature* **1999**, *397*, 601. (c) Tuckerman, M. E.; Marx, D.; Klein, M. L.; Parrinello, M. *Nature* **1997**, *275*, 817.
- (3) (a) Wei, D.; Salahub, D. R. *J. Chem. Phys.* **1997**, *106*, 6086. (b) Schmitt, U. W.; Voth, G. A. *J. Chem. Phys.* **1999**, *111*, 9361. (c) Kim, J.; Schmitt, U. W.; Gruetzmacher, J. A.; Voth, G. A.; Scherer, N. E. *J. Chem. Phys.* **1999**, *111*, 9361. (d) Mella, M.; Clary, D. C. *J. Chem. Phys.* **2003**, *119*, 10048. (e) Iyengar, S. S.; Petersen, M.; Day, T. J. F.; Burnham, C. J.; Teige, V. E.; Voth, G. A. *J. Chem. Phys.* **2005**, *123*, 084309. (f) Lee, H. M.; Tarakeshwar, P.; Park, J. W.; Kolaski, M. R.; Yoon, Y. J.; Yi, H.-B.; Kim, W. Y.; Kim, K. S. *J. Phys. Chem. A* **2004**, *108*, 2949. (g) Christie, R. A.; Jordan, K. D. *J. Phys. Chem. B* **2002**, *106*, 8376. (h) Mella, M.; Kuo, J.-L.; Clary, D. C.; Klein, M. L. *Phys. Chem. Chem. Phys.* **2005**, *7*, 2324. (i) Svanberg, M.; Pettersson, J. B. C. *J. Phys. Chem. A* **1998**, *102*, 1865. (j) Shin, I.; Park, M.; Min, S. K.; Lee, E. C.; Suh, S. B.; Kim, K. S. *J. Chem. Phys.* **2006**, *125*, 234305. (k) Newton, M. D.; Ehrenson, S. *J. Am. Chem. Soc.* **1971**, *93*, 4971. (l) Dai, J.; Zlatko, B.; Huang, X.; Carter, S.; Bowman, J. M. *J. Chem. Phys.* **2003**, *119*, 6571.
- (4) Singh, N. J.; Park, M.; Min, S. K.; Suh, S. B.; Kim, K. S. *Angew. Chem., Int. Ed.* **2006**, *45*, 3795; *Angew. Chem.* **2006**, *118*, 3879.
- (5) (a) Headrick, J. M.; Diken, E. G.; Walters, R. S.; Hammer, N. I.; Christie, R. A.; Cui, J.; Myshakin, E. M.; Duncan, M. A.; Johnson, M. A.; Jordan, K. D. *Science* **2005**, *308*, 1765. (b) Headrick, J. M.; Bopp, J. C.; Johnson, M. A. *J. Chem. Phys.* **2004**, *121*, 11523. (c) Hammer, N. I.; Diken, E. G.; Roscioli, J. R.; Johnson, M. A.; Myshakin, E. M.; Jordan, K. D.; McCoy, A. B.; Huang, X.; Bowman, J. M.; Carter, S. *J. Chem. Phys.* **2005**, *122*, 244301.
- (6) Asmis, K. N.; Pivonka, N. L.; Santambrogio, G.; Brümmer, M.; Kaposta, C.; Neumark, D. M.; Wöste, L. *Science* **2003**, *299*, 1375.
- (7) Fridgen, T. D.; McMahon, T. B.; MacAleese, L.; Lemaire, J.; Maitre, P. *J. Phys. Chem. A* **2004**, *108*, 9008.
- (8) (a) Jiang, J.-C.; Wang, Y.-S.; Chang, H.-C.; Lin, S. H.; Lee, Y. T.; Niedner-Schatteburg, G.; Chang, H.-C. *J. Am. Chem. Soc.* **2000**, *122*, 1398. (b) Yeh, L. I.; Okumura, M. J.; Myers, J. D.; Price, J. M.; Lee, Y. T. *J. Chem. Phys.* **1989**, *91*, 7319. (c) Okumura, M. J.; Yeh, L. I.; Myers, J. D.; Lee, Y. T. *J. Chem. Phys.* **1990**, *94*, 3416. (d) Schwartz, H. A. *J. Chem. Phys.* **1977**, *67*, 1977.
- (9) (a) Miyazaki, M.; Fujii, A.; Ebata, T.; Mikami, N. *Science* **2004**, *304*, 1134. (b) Shin, J. W.; Hammer, N. I.; Diken, E. G.; Johnson, M. A.; Walters, R. S.; Jaeger, T. D.; Duncan, M. A.; Christie, R. A.; Jordan, K. D. *Science* **2004**, *304*, 1140. (c) Wu, C.-C.; Lin, C.-K.; Chang, H.-C.; Jiang, J.-C.; Kuo, J.-L.; Klein, M. L. *J. Chem. Phys.* **2005**, *122*, 074315.
- (10) (a) Brutschy, B. *Chem. Rev.* **2000**, *100*, 3891. (b) Buck, U.; Huisken, F. *Chem. Rev.* **2000**, *100*, 3863. (c) Kim, K. S.; Tarakeshwar, P.; Lee, J. Y. *Chem. Rev.* **2000**, *100*, 4145. (d) Kim, J.; Kim, K. S. *J. Chem. Phys.* **1998**, *109*, 5886. (e) Lee, H. M.; Suh, S. B.; Lee, J. Y.; Tarakeshwar, P.; Kim, K. S. *J. Chem. Phys.* **2000**, *112*, 9759. (f) Hammer, N. I.; Shin, J. W.; Headrick, J. M.; Diken, E. G.; Roscioli, J. R.; Weddell, G. H.; Johnson, M. A. *Science* **2004**, *306*, 675. (g) Patwari, G. N.; Lisy, J. M. *J. Chem. Phys.* **2003**, *118*, 8555.
- (11) Hütter, J.; Alavi, A.; Deutsch, T.; Bernasconi, M.; Focher, P.; Fois, E.; Goedecker, S.; Marx, D.; Tuckerman, M.; Parrinello, M. et al. *CPMD version 3.9.2*; IBM Research Division, MPI Festkörperforschung: Stuttgart, Germany, 1990–2005.
- (12) Eigen, M. *Angew. Chem. Int. Ed.* **1964**, *3*, 1.
- (13) Zundel, G.; Metzger, H. *Z. Phys. Chem.* **1968**, *58*, 225.
- (14) (a) Becke, A. D. *Phys. Rev. A: At., Mol., Opt. Phys.* **1988**, *38*, 3098. (b) Lee, C.; Yang, W.; Parr, R. G. *Phys. Rev. B: Condens. Mater.* **1988**, *37*, 785.
- (15) Frisch, M. J.; Trucks, G. W.; Schlegel, H. B.; Scuseria, G. E.; Robb, M. A.; Cheeseman, J. R.; Montgomery, J. A., Jr.; Vreven, T.; Kudin, K. N.; Burant, J. C.; Millam, J. M.; Iyengar, S. S.; Tomasi, J.; Barone, V.; Mennucci, B.; Cossi, M.; Scalmani, G.; Rega, N.; Petersson, G. A.; Nakatsuji, H.; Hada, M.; Ehara, M.; Toyota, K.; Fukuda, R.; Hasegawa, J.; Ishida, M.; Nakajima, T.; Honda, Y.; Kitao, O.; Nakai, H.; Klene, M.; Li, X.; Knox, J. E.; Hratchian, H. P.; Cross, J. B.; Bakken, V.; Adamo, C.; Jaramillo, J.; Gomperts, R.; Stratmann, R. E.; Yazyev, O.; Austin, A. J.; Cammi, R.; Pomelli, C.; Ochterski, J. W.; Ayala, P. Y.; Morokuma, K.; Voth, G. A.; Salvador, P.; Dannenberg, J. J.; Zakrzewski, V. G.; Dapprich, S.; Daniels, A. D.; Strain, M. C.; Farkas, O.; Malick, D. K.; Rabuck, A. D.; Raghavachari, K.; Foresman, J. B.; Ortiz, J. V.; Cui, Q.; Baboul, A. G.; Clifford, S.; Cioslowski, J.; Stefanov, B. B.; Liu, G.; Liashenko, A.; Piskorz, P.; Komaromi, I.; Martin, R. L.; Fox, D. J.; Keith, T.; Al-Laham, M. A.; Peng, C. Y.; Nanayakkara, A.; Challacombe, M.; Gill, P. M. W.; Johnson, B.; Chen, W.; Wong, M. W.; Gonzalez, C.; Pople, J. A. *Gaussian 03*, revision B1; Gaussian, Inc.: Wallingford, CT, 2004.
- (16) Chanban, G. M.; Jung, J. O.; Gerber, R. B. *J. Chem. Phys.* **1999**, *111*, 1823.
- (17) Werner, H.-J.; Knowles, P. J.; Amos, R. D.; Bernhardsson, A.; Berning, A.; Celani, P.; Cooper, D. L.; Deegan, M. J. O.; Dobbyn, A. J.; Eckert, F.; Hampel, C.; Hetzer, G.; Korona, T.; Lindh, R.; Lloyd, A. W.; McNicholas, S. J.; Manby, F. R.; Meyer, W.; Mura, M. E.; Nicklass, A.; Palmieri, P.; Pitzer, R.; Rauhut, G.; Schütz, M.; Schumann, U.; Stoll, H.; Stone, A. J.; Tarroni, R.; Thorsteinsson, T. *MOLPRO*, 2002.6; University of Birmingham: Birmingham, England, 2002.
- (18) Lee, S. J.; Chung, H. Y.; Kim, K. S. *Bull. Korean Chem. Soc.* **2004**, *25*, 1061.
- (19) Martyna, G. J.; Tuckerman, M. E. *J. Chem. Phys.* **1999**, *110*, 2810.
- (20) (a) Trouiller, N.; Martins, J. L. *Phys. Rev. B: Condens. Mater.* **1991**, *43*, 1993. (b) Sprik, M.; Hutter, J.; Parrinello, M. *J. Chem. Phys.* **1996**, *105*, 1142.
- (21) Nos'e, S. *J. Chem. Phys.* **1984**, *81*, 511. (b) Nos'e, S. *Mol. Phys.* **1984**, *52*, 255. (c) Hoover, W. G. *Phys. Rev. A: At., Mol., Opt. Phys.* **1985**, *31*, 1695.
- (22) Odutola, J. A.; Dyke, T. R. *J. Chem. Phys.* **1980**, *72*, 5062. (b) Kim, K. S.; Mhin, B. J.; Choi, U.-S.; Lee, K. J. *J. Chem. Phys.* **1992**, *97*, 6649. (c) Lee, H. M.; Suh, S. B.; Lee, J. Y.; Tarakeshwar, P.; Kim, K. S. *J. Chem. Phys.* **2000**, *112*, 9759.
- (23) Benedict, W. S.; Gailar, N.; Plyler, E. K. *J. Chem. Phys.* **1956**, *24*, 1139.
- (24) Gaigeot, M. P.; Vuilleumier, R.; Sprik, M.; Borgis, D. *J. Chem. Theory Comput.* **2005**, *1*, 772.
- (25) (a) Begemann, M. H.; Gudeman, C. S.; Pfaff, J.; Saykally, R. J. *Phys. Rev. Lett.* **1983**, *51*, 554. (b) Tang, J.; Oka, T. *J. Mol. Spectrosc.* **1999**, *196*, 120. (c) Gruebele, M.; Polak, M.; Saykally, R. J. *J. Chem. Phys.* **1987**, *87*, 3347. (d) Liu, D.-J.; Haese, N. N.; Oka, T. *J. Chem. Phys.* **1985**, *82*, 5368.
- (26) (a) Xie, Y.; Remington, R. B.; Schaefer, H. F., III. *J. Chem. Phys.* **1994**, *101*, 4878. (b) Valeev, E. F.; Schaefer, H. F., III. *J. Chem. Phys.* **1998**, *108*, 7197. (c) Klein, S.; Kochanski, E.; Strich, A.; Sadlej, A. J. *J. Phys. Chem. A* **1997**, *101*, 4799. (d) Huang, X.; Cho, H. M.; Carter, S.; Ojamae, L.; Bowman, J. M.; Singer, S. J. *J. Phys. Chem. A* **2003**, *107*, 7142. (e) Verner, M. V.; Kuhn, O.; Sauer, J. *J. Chem. Phys.* **2001**, *114*,

240. (f) Cho, H. M.; Singer, S. J. *J. Phys. Chem. A* **2004**, *108*, 8691. (g) Sauer, J.; Dobler, J. *ChemPhysChem* **2005**, *6*, 1706. (h) Dai, J.; Bacic, Z.; Huang, X.; Carter, S.; Bowman, J. M. *J. Chem. Phys.* **2003**, *119*, 6571. (i) Kaledin, M.; Kaledin, A. L.; Bowman, J. M. *J. Phys. Chem. A* **2006**, *110*,

2933. (j) Cheng, H.-P.; Krause, J. L. *J. Chem. Phys.* **1997**, *107*, 8461. (k) Cheng, H.-P. *J. Phys. Chem.* **1998**, *102*, 6201.

(27) Kim, J.; Lee, H. M.; Suh, S. B.; Majumdar, D.; Kim, K. S. *J. Chem. Phys.* **2000**, *113*, 5259.